TABLE OF CONTENT

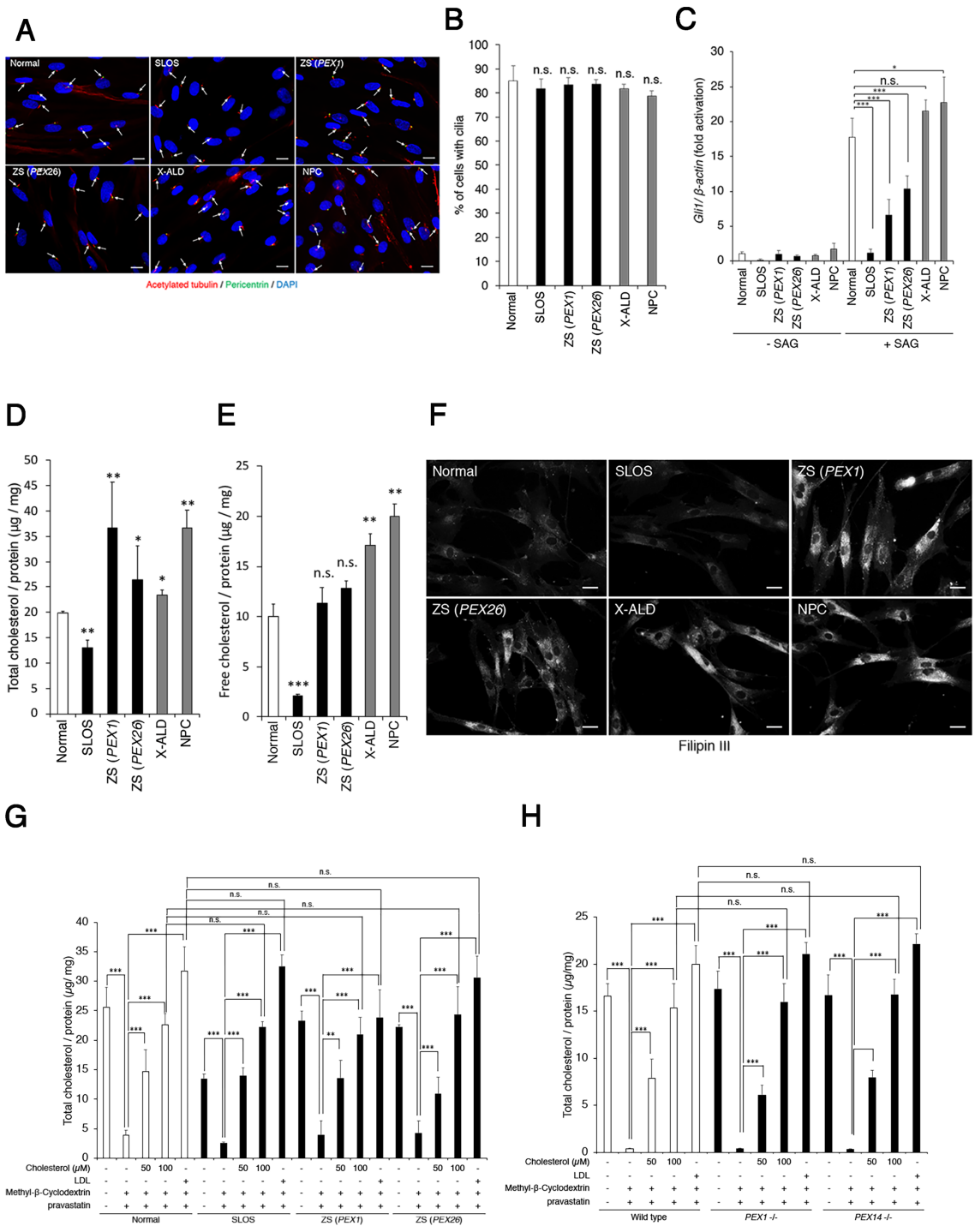

Appendix Fig. S1. Cholesterol is massively accumulated in the cytoplasm of ZS patient cells

(A) Primary fibroblasts from a normal individual and patients were cultured without serum for 24 h and then immunostained with anti-acetylated tubulin (red) and anti-pericentrin (green) antibodies. DNA was stained with DAPI (blue). Arrows indicate primary cilia. Scale bar, 5 μm.

(B) Quantification of the percentage of ciliated cells from (A). Ciliogenesis in the patient cells was not significantly altered from that of normal individual cells (one-way ANOVA with Tukey's HSD, n=3: >200 cells per experiment).

(C) Primary fibroblasts from a normal individual and the cases with syndromes were treated with 1 μM SAG or vehicle (DMSO) for 24 h, and the levels of transcripts of the Shh target gene *Gli1* and the reference gene *β-actin* were measured by qRT-PCR. Error bars indicate s.d. of three independent experiments (*p<0.05, ***p<0.001: one-way ANOVA with Tukey's HSD, n=3: triplicates per trial).

(D) Total cellular cholesterol levels in the quiescent G_0-phase skin primary fibroblasts. Results are presented as the mean ± s.d. of three independent trials (*p<0.05, **p<0.01: one-way ANOVA with Tukey's HSD, n=3: triplicates per trial).

(E) Cellular free-cholesterol levels in the quiescent G_0-phase skin primary fibroblasts. Results are presented as the mean ± s.d. of three independent trials (**p<0.01, ***p<0.001: one-way ANOVA with Tukey's HSD, n=3: triplicates per trial).

(F) Cholesterol in the primary skin fibroblasts from a normal individual, SLOS patient, ZS patients, X-ALD patient, and NPC patient was stained with Filipin III (white). The severe intracellular accumulation of cholesterol was observed in cells from the ZS, X-ALD, and NPC patients. Scale bar, 5 μm.

(G) Total cellular cholesterol levels in the skin primary fibroblasts treated with cholesterol/methyl-β-cyclodextrin complex or LDL. Results are presented as the mean ± s.d. of three independent trials (**p<0.01, ***p<0.001: one-way ANOVA with Tukey's HSD, n=3: triplicates per trial).

(H) Total cellular cholesterol levels in the hTERT-RPE1 cell lines treated with cholesterol/methyl-β-cyclodextrin complex or LDL. Results are presented as the mean ± s.d. of three independent trials (***p<0.001: one-way ANOVA with Tukey's HSD, n=3: triplicates per trial).

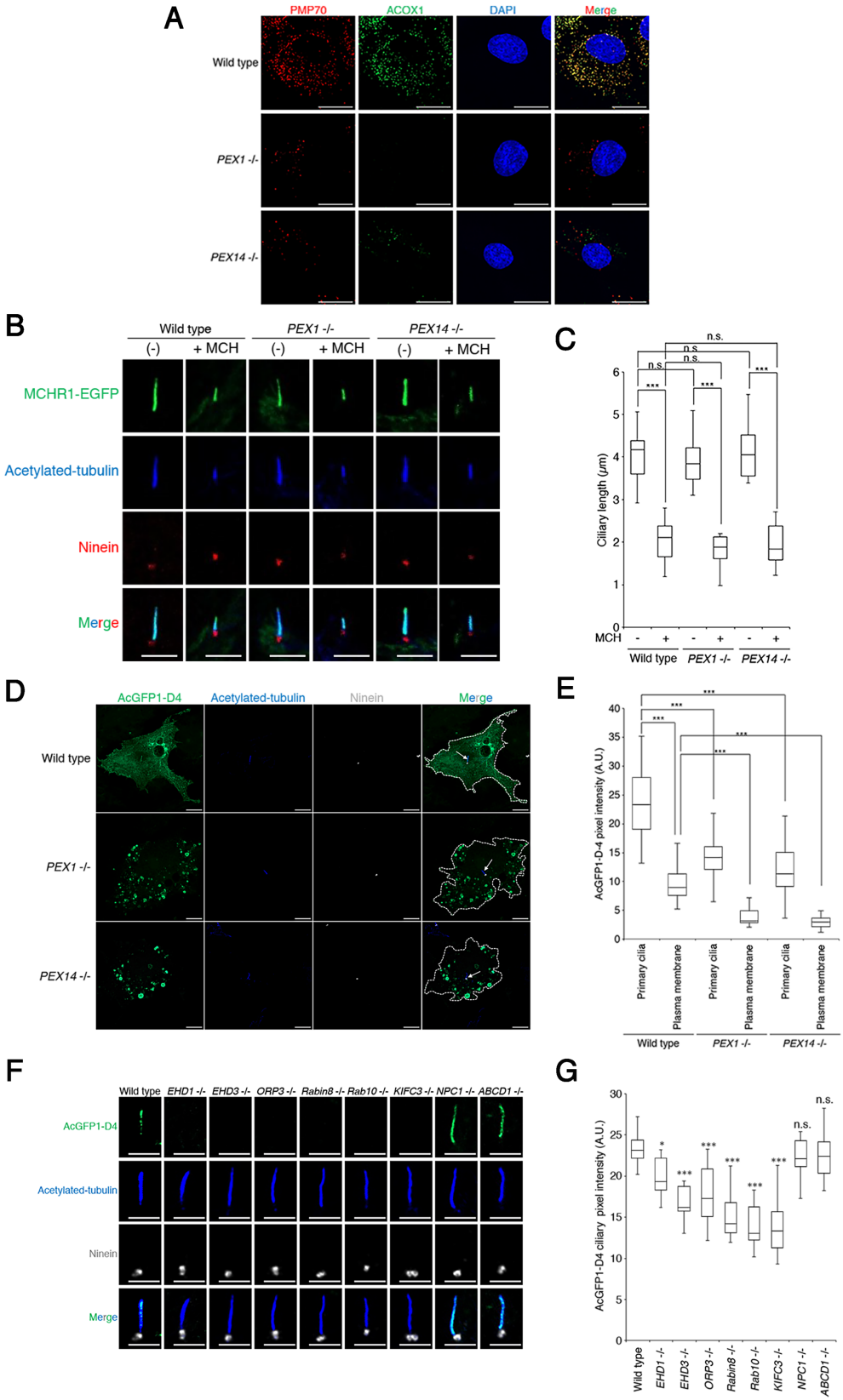

Appendix Fig. S2. The ciliary cholesterol defects in *PEX1*$^{-/-}$ and *PEX14*$^{-/-}$ hTERT-RPE1 cells

(A) Immunostaining with anti-PMP70 (red) and anti-ACOX1 (green) in wild-type, *PEX1*$^{-/-}$, and

PEX14$^{-/-}$ hTERT-RPE1 cells. DNA was stained with DAPI (blue), showing that PMP70 and ACOX1-double-positive peroxisomes were remarkably reduced in *PEX1*$^{-/-}$and *PEX14*$^{-/-}$ hTERT-RPE1 cells. Scale bar, 10 μm.

(B) Quiescent G_0-phase wild-type, *PEX1*$^{-/-}$, and *PEX14*$^{-/-}$ hTERT-RPE1 cells transfected with MCHR1-EGFP were treated with or without 1 μM MCH for 6 h, and then immunostained with anti-GFP (green), anti-acetylated-tubulin (blue), and anti-ninein (red) antibodies. Scale bar, 5 μm.

(C) Quantification of the ciliary length in wild-type, *PEX1*$^{-/-}$, and *PEX14*$^{-/-}$ hTERT-RPE1 cells transfected with MCHR1-EGFP from (B). The MCH-dependent ciliary shortening in *PEX1*$^{-/-}$ and *PEX14*$^{-/-}$ hTERT-RPE1 cells exhibited no significant alterations compared to that of wild-type hTERT REPE1 cells (***p<0.001: one-way ANOVA with Tukey's HSD, n=3: 90–100 cells per experiment).

(D) Quiescent G_0-phase wild-type, *PEX1*$^{-/-}$, and *PEX14*$^{-/-}$ hTERT-RPE1 cells transfected with AcGFP1-tagged Domain 4 (D4) of Perfringolysin O (green) as a cholesterol probe were immunostained with anti-pericentrin (white) and anti-acetylated tubulin (blue) antibodies. Arrows indicate primary cilia. Dotted line traces the border of cells surrounded by plasma membrane. Scale bar, 5 μm.

(E) Quantification of the AcGFP1-tagged D4 intensity at primary cilia and plasma membranes from (D). The ciliary signal of AcGFP1-tagged D4 was more enhanced than that of plasma membrane in the parental hTERT-RPE1 cells. In addition, the ciliary and plasma membranous signals in *PEX1*$^{-/-}$ and *PEX14*$^{-/-}$ hTERT-RPE1 cells were significantly diminished (***p<0.001: one-way ANOVA with Tukey's HSD, n=3: 35–40 cells per experiment).

(F) Quiescent G_0-phase wild-type, *EHD1*$^{-/-}$, *EHD3*$^{-/-}$, *ORP3*$^{-/-}$, *Rabin8*$^{-/-}$, *Rab10*$^{-/-}$, *KIFC3*$^{-/-}$, *NPC1*$^{-/-}$, and *ABCD1*$^{-/-}$ hTERT-RPE1 cells transfected with AcGFP1-tagged D4 (green) were immunostained with anti-ninein (white) and anti-acetylated tubulin (blue) antibodies. Scale bar, 5 μm.

(G) Quantification of the AcGFP1-tagged D4 intensity at primary cilia from (F). The ciliary signal of AcGFP1-tagged D4 in *EHD1*$^{-/-}$, *EHD3*$^{-/-}$, *ORP3*$^{-/-}$, *Rabin8*$^{-/-}$, *Rab10*$^{-/-}$, and *KIFC3*$^{-/-}$ hTERT-RPE1 cells was significantly diminished (*p<0.05, ***p<0.001: one-way ANOVA with Tukey's HSD, n=3: 25–30 cells per experiment).

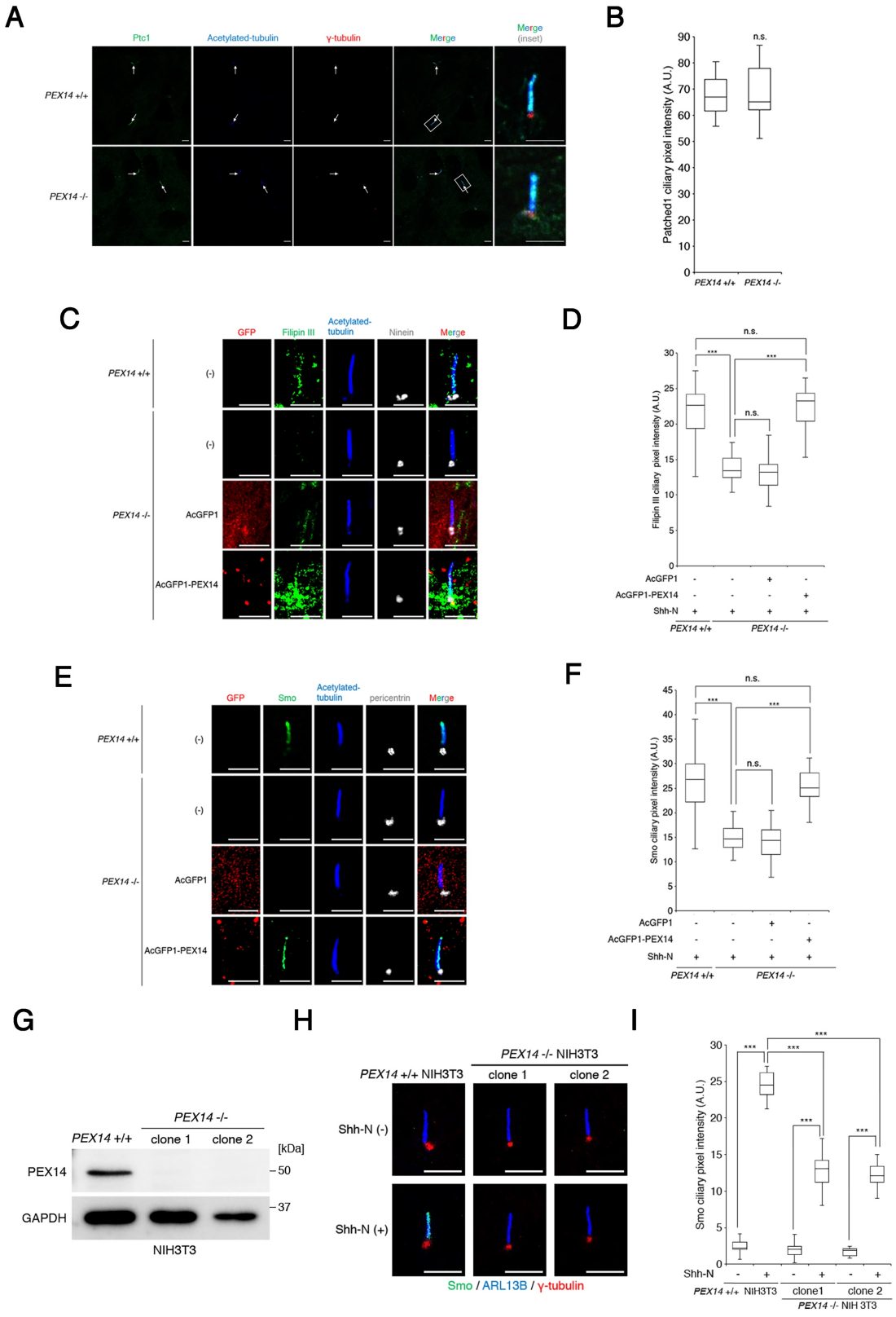

Appendix Fig. S3. The exogenous *PEX14* cDNA expression rescues the ciliary defects in *PEX14*$^{-/-}$ hTERT-RPE1 cells

(A) Immunostaining with anti-Ptc1 (green) anti-acetylated-tubulin (blue), and anti-γ-tubulin (red) in wild-type and *PEX14*$^{-/-}$ hTERT-RPE1 cells in quiescent G_0 phase. Arrows indicate primary cilia. Scale bar, 5μm.

(B) Quantification of the Ptc1 intensity at primary cilia from (A). Wild-type and *PEX14*$^{-/-}$hTERT-RPE1 cells had no significant alterations in the ciliary signal of Ptc1 (***p<0.001: one-way ANOVA with Tukey's HSD, n=3: 40–50 cells per experiment).

(C) Quiescent G_0-phase *PEX14*$^{-/-}$ hTERT-RPE1 cells transfected with AcGFP1 (red) or AcGFP1-tagged PEX14 (red) were immunostained with anti-acetylated-tubulin (blue) and anti-ninein (white) antibodies. Cholesterol was stained with Filipin III (Green). The scale bars represent 5 μm.

(D) Quantification of (C) showing that AcGFP1-tagged PEX14 effectively restored the defect in ciliary enrichment of cholesterol in *PEX14*$^{-/-}$ hTERT-RPE1 cells (***p<0.001: one-way ANOVA with Tukey's HSD, n=3: 35–40 cells per experiment).

(E) Quiescent G_0-phase *PEX14*$^{-/-}$ hTERT-RPE1 cells transfected with AcGFP1 (red) or AcGFP1-tagged PEX14 (red) were stimulated with Shh-N for 24 h, and then immunostained with anti-Smo (green), anti-acetylated-tubulin (blue), and anti-pericentrin (white) antibodies. The scale bars represent 5 μm.

(F) Quantification of (E) showing that AcGFP1-tagged PEX14 effectively rescued the defect in Shh-N-mediated ciliary Smo accumulation in *PEX14*$^{-/-}$ hTERT-RPE1 cells (***p<0.001: one-way ANOVA with Tukey's HSD, n=3: 35–40 cells per experiment).

(G) Western blot analysis showing depletion of PEX14 in the *PEX14*$^{-/-}$ NIH3T3 cell clones. GAPDH served as a loading control.

(H) Quiescent G_0-phase *PEX14*$^{-/-}$ NIH3T3 cells were stimulated with Shh-N for 24 h, and then immunostained with anti-Smo (green), anti-ARL13B (blue), and anti-γ-tubulin (red) antibodies. The scale bars represent 5 μm.

(I) Quantification of (H) showing the defect in Shh-N-mediated ciliary Smo accumulation in the *PEX14*$^{-/-}$ NIH3T3 cell clones (***p<0.001: one-way ANOVA with Tukey's HSD, n=3: 35–40 cells per experiment).

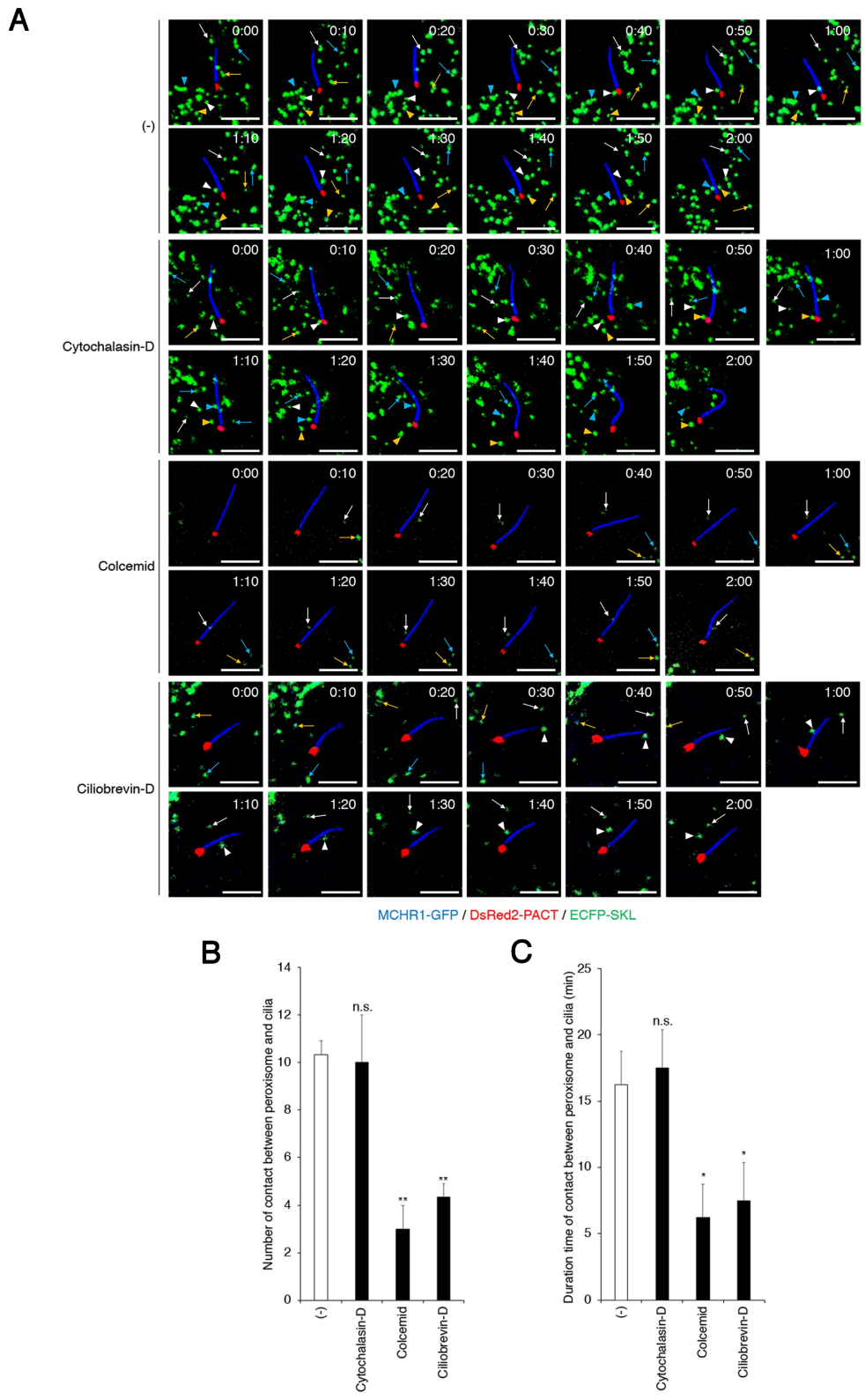

Appendix Fig. S4. Microtubules are necessary for the interaction between peroxisomes and primary cilia

(A) MCHR1-GFP (blue)-/DsRed2-PACT (red)-constitutively expressing hTERT-RPE1 cells transiently expressing the peroxisomal marker ECFP-SKL (green) were serum-starved for 24 h, and then treated with Colcemid, Cytochalasin-D, or Ciliobrevin-D for 4 h. They were imaged live for 2 h by confocal microscopy (Movie EV1–4). Arrowheads represent the peroxisomes interacting with primary cilia, while arrows show the peroxisomes without any contact with cilia. Scale bar, 5 μm.

(B) Quantification of (A) showing that colcemid and Ciliobrevin-D significantly decreased the number of spatial interactions between peroxisomes and primary cilia for 2 h (**$p<0.01$: one-way ANOVA with Tukey's HSD, n=3: 45–50 peroxisomes per experiment).

(C) Quantification of (A) indicating that colcemid and Ciliobrevin-D significantly shortened the duration of spatial communication between peroxisomes and primary cilia (*$p<0.05$: one-way ANOVA with Tukey's HSD, n=3: 45–50 peroxisomes per experiment).

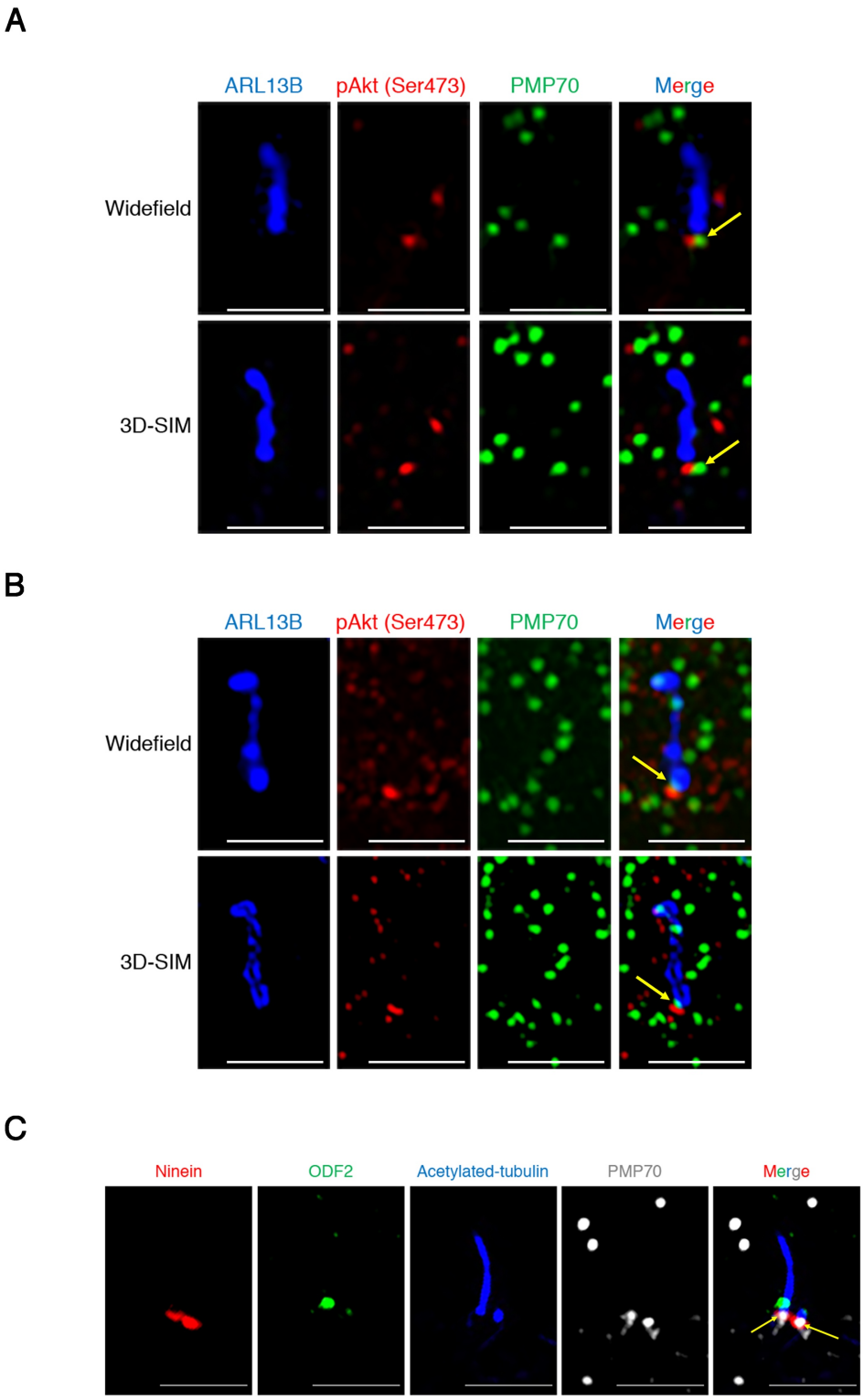

Appendix Fig. S5. Three-dimensional structured illumination (3D-SIM) microcopy reveals the spatial interaction between peroxisomes and primary cilia

Quiescent G_0-phase wild-type hTERT-RPE1 cells were immunostained with anti-ARL13B (blue), anti-phospho-S473-Akt (red), and anti-PMP70 (green) antibodies.

(A) The widefield images (upper panels) and 3D-SIM images (lower panels) were obtained using a Zeiss ELYRA microscope.

(B) The widefield images (upper panels) and 3D-SIM images (lower panels) were captured using a DeltaVision OMX SR microscope. Arrows indicate the peroxisomes interacting with the ciliary pocket. Scale bar, 2.5 μm.

(C) Confocal images of the quiescent G_0-phase hTERT-RPE1 cells immunostained with anti-ninein (red), anti-ODF2 (green), anti-acetylated-tubulin (blue), and anti-PMP70 (white) antibodies indicate that the cilium-bound peroxisomes (yellow arrows) did not contact the distal appendages labeled with the ODF2 signals. The scale bars indicate 5 μm.

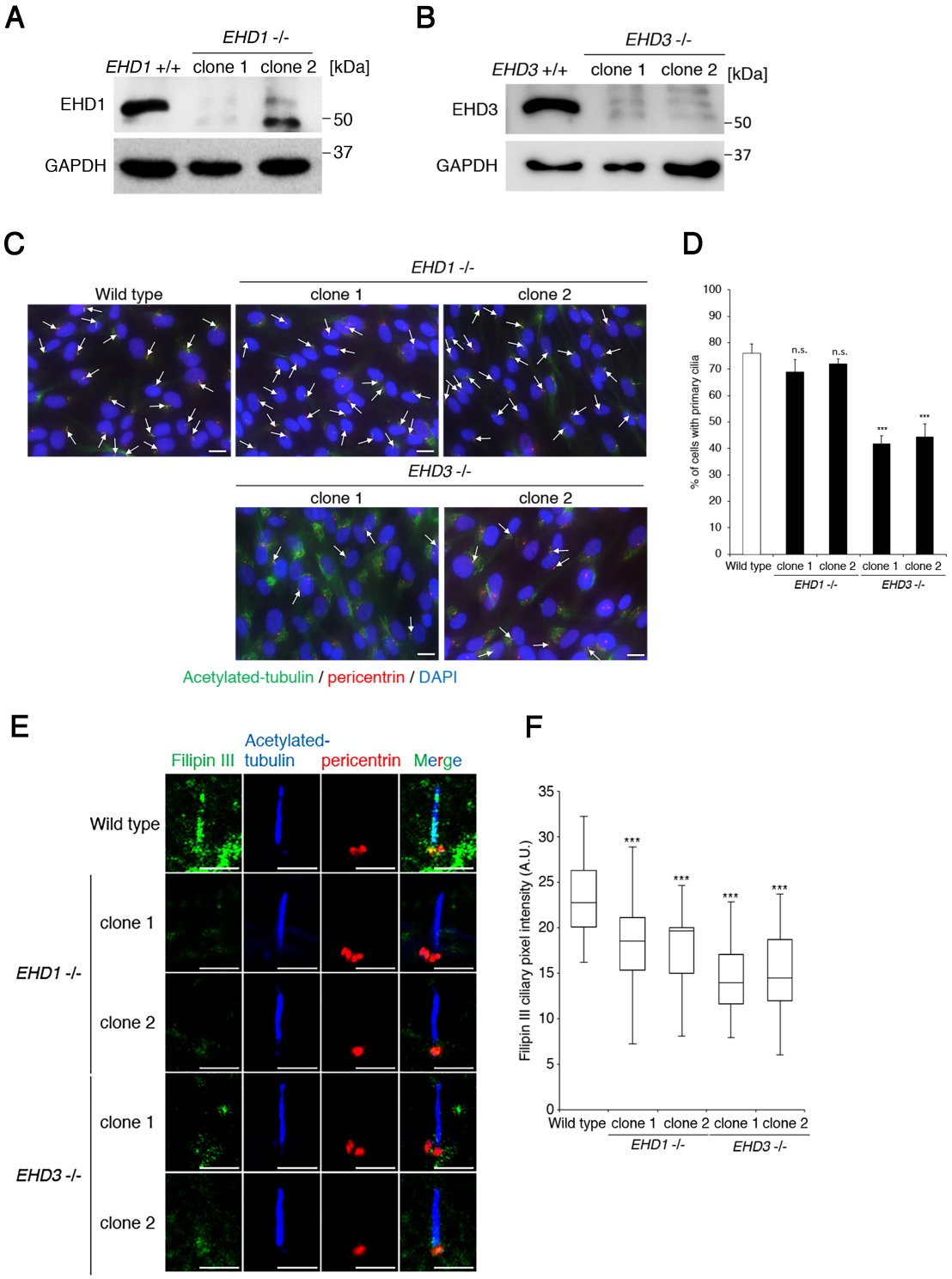

Appendix Fig. S6. The ciliary cholesterol supply is impaired in *EHD1*$^{-/-}$ and *EHD3*$^{-/-}$ hTERT-RPE1 cells

(A) Western blot analysis showing the depletion of EHD1 in the *EHD1*$^{-/-}$ hTERT-RPE1 cell clones. GAPDH served as a loading control.

(B) Western blot analysis showing the depletion of EHD3 in the *EHD3*$^{-/-}$ hTERT-RPE1 cell clones. GAPDH served as a loading control.

(C) Wild-type, *EHD1*$^{-/-}$, and *EHD3*$^{-/-}$ hTERT-RPE1 cells were cultured without serum for 24 h and then immunostained with anti-acetylated tubulin (green) and anti-pericentrin (red) antibodies. DNA was stained with DAPI (blue). Arrows indicate primary cilia. Scale bar, 15 μm.

(D) Quantification of the proportion of ciliated cells from (C) indicating that ciliogenesis in the *EHD3*$^{-/-}$ hTERT-RPE1 cell clones was significantly reduced compared with that of wild-type and *EHD1*$^{-/-}$ cells (***$p<0.001$: one-way ANOVA with Tukey's HSD, n=3: 100–120 cells per experiment).

(E) Wild-type, *EHD1*$^{-/-}$, and *EHD3*$^{-/-}$ hTERT-RPE1 cells incubated for 24 h without serum were immunostained with anti-pericentrin (red) and anti-acetylated-tubulin (blue) antibodies. Cholesterol was stained with Filipin III (green). Scale bar, 5 μm.

(F) Quantification of (E) indicating that *EHD1*$^{-/-}$ and *EHD3*$^{-/-}$ hTERT-RPE1 cells significantly reduced the ciliary accumulation of cholesterol (***$p<0.01$: one-way ANOVA with Tukey's HSD, n=3: 40–50 cells per experiment).

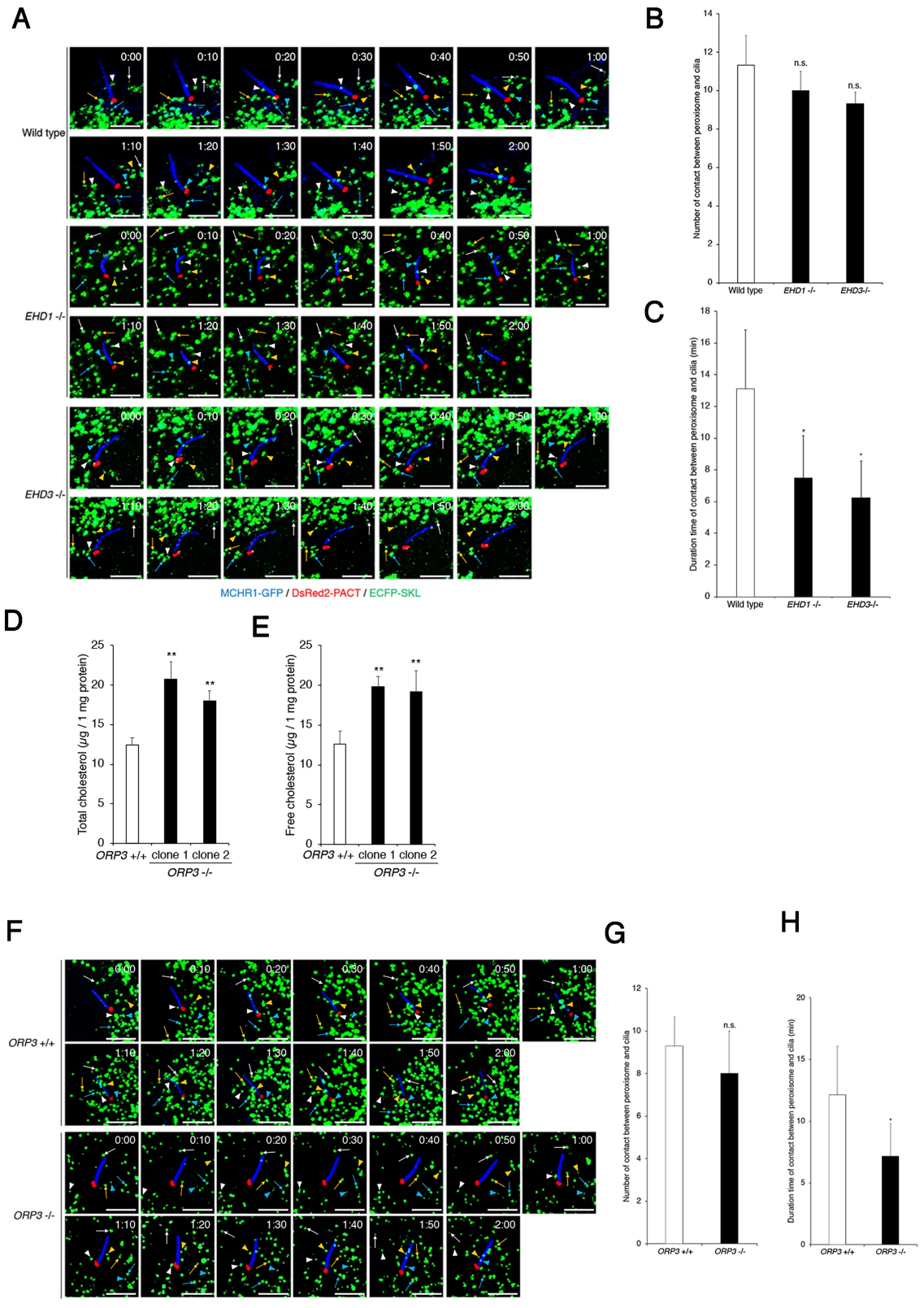

Appendix Fig. S7. The contact between peroxisomes and primary cilia is impaired in *EHD3*$^{-/-}$

and *ORP3*$^{-/-}$ hTERT-RPE1 cells

(A) Quiescent G_0-phase wild-type, *EHD1*$^{-/-}$ and *EHD3*$^{-/-}$ hTERT-RPE1 cells transiently expressing MCHR1-GFP, DsRed2-PACT, and ECFP-SKL were imaged live for 2 h by confocal microscopy (Movie EV5–7). Arrowheads represent the peroxisomes interacting with primary cilia, while arrows show the peroxisomes without any contact with cilia. Scale bar, 5 μm.

(B) Quantification of (A) showing that disruption of the *EHD1* and *EHD3* genes did not alter the number of spatial interactions between peroxisomes and primary cilia for 2 h (one-way ANOVA with Tukey's HSD, n=3: 45–50 peroxisomes per experiment).

(C) Quantification of (A) indicating that disruption of the *EHD3* gene but not the *EHD1* gene significantly shortened the duration of spatial communication between peroxisomes and primary cilia (*$p<0.05$: one-way ANOVA with Tukey's HSD, n=3: 45–50 peroxisomes per experiment).

(D) Total cellular cholesterol levels in the quiescent G_0-phase *ORP3*$^{+/+}$ and *ORP3*$^{-/-}$ hTERT-RPE1 cells. Results are presented as the mean ± s.d. of three independent trials (**$p<0.05$: one-way ANOVA with Tukey's HSD, n=3: triplicates per trial).

(E) Cellular free-cholesterol levels in in the quiescent G_0-phase *ORP3*$^{+/+}$ and *ORP3*$^{-/-}$ hTERT-RPE1 cells. Results are presented as the mean ± s.d. of three independent trials (**$p<0.05$: one-way ANOVA with Tukey's HSD, n=3: triplicates per trial).

(F) Quiescent G_0-phase *ORP3*$^{+/+}$ and *ORP3*$^{-/-}$ hTERT-RPE1 cells transiently expressing MCHR1-GFP, DsRed2-PACT, and ECFP-SKL were imaged live for 2 h by confocal microscopy (Movie EV8 and 9). Arrowheads represent the peroxisomes interacting with primary cilia, while arrows show the peroxisomes without any contact with cilia. Scale bar, 5 μm.

(G) Quantification of (F) showing that disruption of the *ORP3* gene did not alter the number of spatial interactions between peroxisomes and primary cilia for 2 h (one-way ANOVA with Tukey's HSD, n=3: 45–50 peroxisomes per experiment).

(H) Quantification of (F) indicating that disruption of the *ORP3* gene significantly shortened the duration of spatial communication between peroxisomes and primary cilia (*$p<0.05$: one-way ANOVA with Tukey's HSD, n=3: 45–50 peroxisomes per experiment).

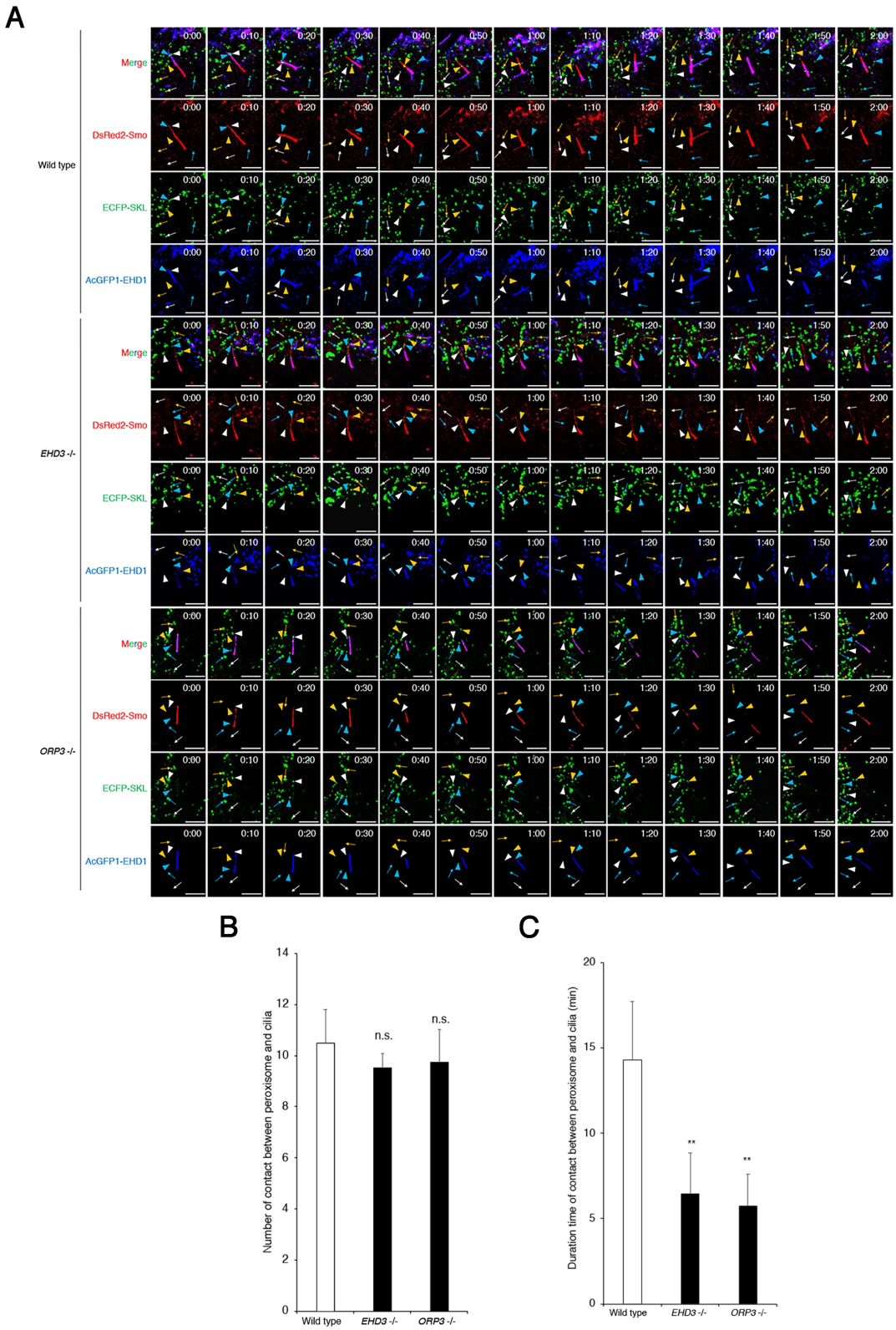

Appendix Fig. S8. The contact between peroxisomes and ciliary pocket is impaired in *EHD3*$^{-/-}$

and *ORP3*$^{-/-}$ hTERT-RPE1 cells

(A) Quiescent G_0-phase wild-type, *EHD3*$^{-/-}$, and *ORP3*$^{-/-}$ hTERT-RPE1 cells transiently expressing AcGFP1-EHD1 (blue), DsRed2-Smo (red), and ECFP-SKL (green) were imaged live for 2 h by confocal microscopy (Movie EV10—12). Arrowheads represent the peroxisomes interacting with the AcGFP1-EHD1-labeled ciliary pocket, while arrows show the peroxisomes without any contact with the ciliary pocket. Scale bar, 5 μm.

(B) Quantification of (A) showing that disruption of the *EHD3* and *ORP3* genes did not alter the number of spatial interactions between peroxisomes and the AcGFP1-EHD1-labeled ciliary pocket for 2 h (one-way ANOVA with Tukey's HSD, n=4: 45–50 peroxisomes per experiment).

(C) Quantification of (A) indicating that disruption of the *EHD3* and *ORP3* genes significantly shortened the duration of spatial communication between peroxisomes and the AcGFP1-EHD1-labeled ciliary pocket (*$p<0.05$: one-way ANOVA with Tukey's HSD, n=7: 45–50 peroxisomes per experiment).

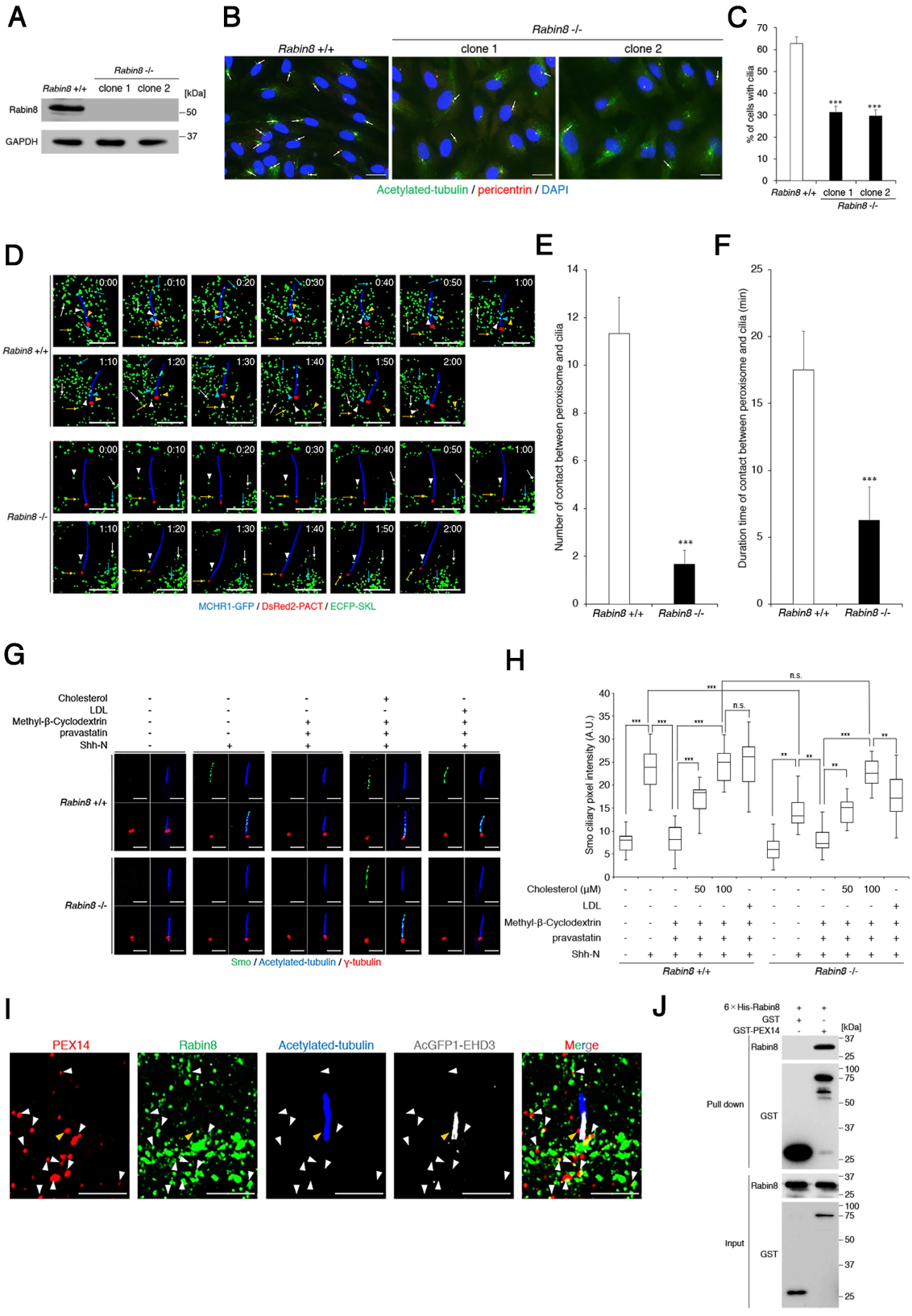

Appendix Fig. S9. The interaction between peroxisomes and primary cilia is impaired in

***Rabin8*$^{-/-}$ hTERT-RPE1 cells**

(A) Western blot analysis showing depletion of Rabin8 in the *Rabin8*$^{-/-}$ hTERT-RPE1 cell clones. GAPDH served as a loading control.

(B) *Rabin8*$^{+/+}$ and *Rabin8*$^{-/-}$ hTERT-RPE1 cells were cultured without serum for 24 h and then immunostained with anti-acetylated tubulin (green) and anti-pericentrin (red) antibodies. DNA was stained with DAPI (blue). Arrows indicate primary cilia. Scale bar, 20 μm.

(C) Quantification of the proportion of ciliated cells from (B) indicating that ciliogenesis in the *Rabin8*$^{-/-}$ hTERT-RPE1 cell clones was significantly reduced compared with that in the *Rabin8*$^{+/+}$ cells (***p<0.001: one-way ANOVA with Tukey's HSD, n=3: 100–120 cells per experiment).

(D) Quiescent G_0-phase *Rabin8*$^{+/+}$ and *Rabin8*$^{-/-}$ hTERT-RPE1 cells transiently expressing MCHR1-GFP, DsRed2-PACT, and ECFP-SKL were imaged live for 2 h by confocal microscopy (Movie EV13 and 14). Arrowheads represent the peroxisomes interacting with primary cilia, while arrows show the peroxisomes without any contact with cilia. Scale bar, 5 μm.

(E) Quantification of (D) showing that disruption of the *Rabin8* gene significantly reduced the number of spatial interactions between peroxisomes and primary cilia for 2 h (***p<0.001: one-way ANOVA with Tukey's HSD, n=3: 45–50 peroxisomes per experiment).

(F) Quantification of (D) indicating that disruption of the *Rabin8* gene significantly shortened the duration of spatial communication between peroxisomes and primary cilia (***p<0.001: one-way ANOVA with Tukey's HSD, n=3: 45–50 peroxisomes per experiment).

(G) Quiescent G_0-phase *Rabin8*$^{+/+}$ and *Rabin8*$^{-/-}$ hTERT-RPE1 cells were treated with or without 1.5% methyl-β-cyclodextrin for 45 min, and then incubated with or without cholesterol (cholesterol/methyl-β-cyclodextrin complex) for 1 h. After removing exogenous cholesterol, they were stimulated with 50 nM Shh-N for 24 h in the presence of pravastatin, and then immunostained with anti-Smo (green), anti-acetylated-tubulin (blue), and anti-γ-tubulin (red) antibodies. For the alternative cholesterol complementation, LDL (0.06 mg/ml) was co-incubated with Shh-N and pravastatin for 24 h after methyl-β-cyclodextrin-mediated cholesterol depletion. Scale bar, 2.5 μm.

(H) Quantification of (G) indicating that exogenous cholesterol (cholesterol/methyl-β-cyclodextrin complex) enabled rescue of the dampened Shh-N-induced ciliary accumulation of Smo in *Rabin8*$^{-/-}$ hTERT-RPE1 cells, while the LDL complementation did not rescue the ciliary phenotypes efficiently (**p<0.01, ***p<0.001: one-way ANOVA with Tukey's HSD, n=3: 45–50 cells per experiment).

(I) Confocal images of the quiescent G_0-phase hTERT-RPE1 cells transfected with AcGFP1-tagged EHD3 (white) immunostained with anti-acetylated-tubulin (blue), anti-PMP70 (red), and anti-Rabin8 (green) antibodies indicate the Rabin8-bound peroxisome (yellow arrowhead) at the ciliary pocket.

The white arrowheads show other Rabin8-bound peroxisomes. The scale bars indicate 2 μm.

(J) Recombinant GST (0.2 μg) or GST fused to PEX14 proteins (1 μg) and 6×His-Rabin8 protein (1 μg) were pulled down using glutathione-Sepharose beads. GST-tagged PEX14 and 6×His-tagged Rabin8 proteins in the pull-down fractions and inputs were detected by western blotting.

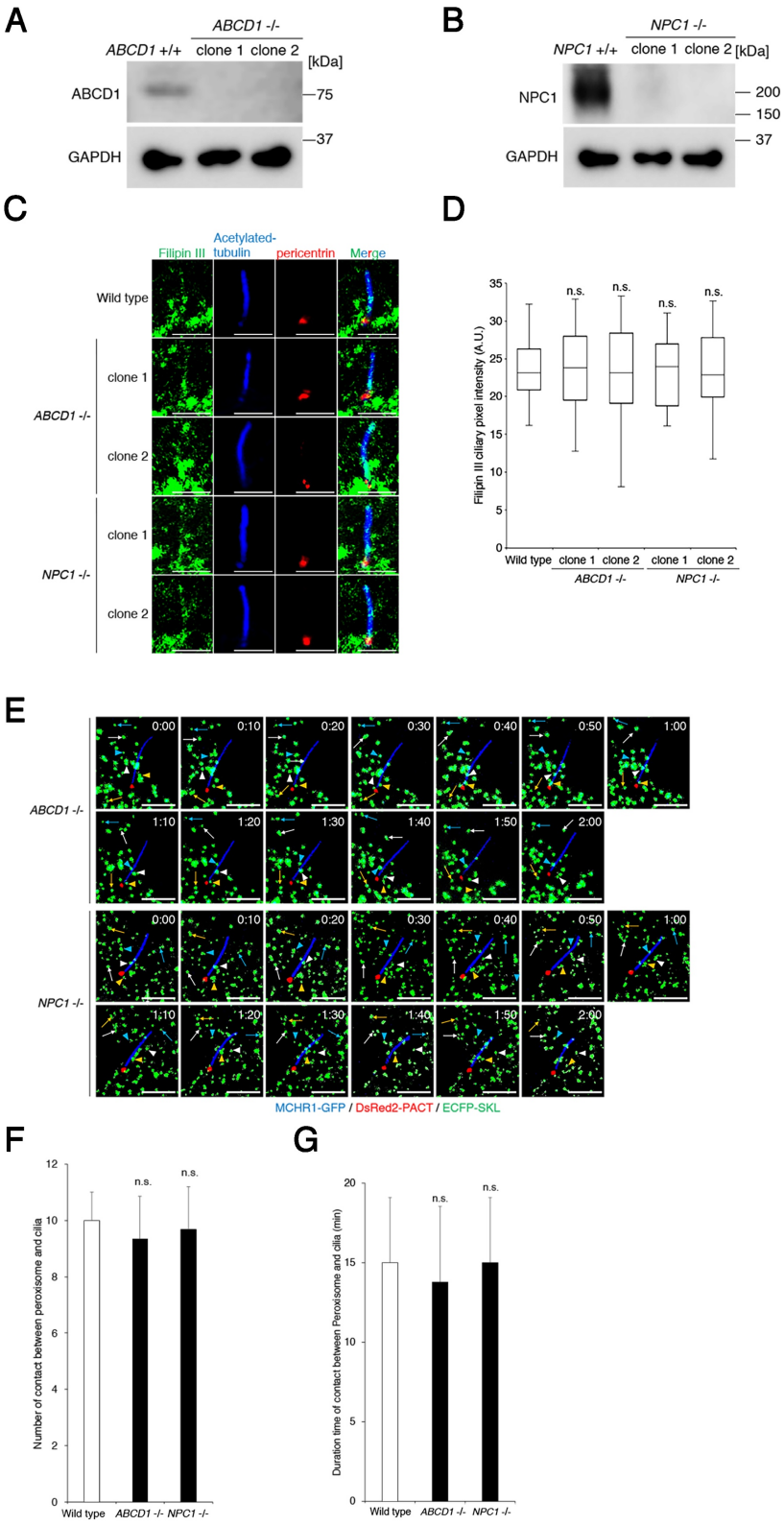

Appendix Fig. S10. *ABCD1*$^{-/-}$ and *NPC1*$^{-/-}$ hTERT-RPE1 cells show the normal dynamics of peroxisomes for communication with primary cilia

(A) Western blot analysis showing the depletion of ABCD1 in the *ABCD1*$^{-/-}$ hTERT-RPE1 cell clones. GAPDH served as a loading control.

(B) Western blot analysis showing the depletion of NPC1 in the *NPC1*$^{-/-}$ hTERT-RPE1 cell clones. GAPDH served as a loading control.

(C) Wild-type, *ABCD1*$^{-/-}$, and *NPC1*$^{-/-}$ hTERT-RPE1 cells incubated for 24 h without serum were immunostained with anti-pericentrin (red) and anti-acetylated-tubulin (blue) antibodies. Cholesterol was stained with Filipin III (green). Scale bar, 5 μm.

(D) Quantification of (C) indicating that *ABCD1*$^{-/-}$ and *NPC1*$^{-/-}$ hTERT-RPE1 cells normally showed the ciliary accumulation of cholesterol (one-way ANOVA with Tukey's HSD, n=3: 45–50 cells per experiment).

(E) Quiescent G_0-phase wild-type, *ABCD1*$^{-/-}$, and *NPC1*$^{-/-}$ hTERT-RPE1 cells transiently expressing MCHR1-GFP (blue), DsRed2-PACT (red), and ECFP-SKL (green) were imaged live for 2 h by confocal microscopy (Movie EV15 and 16). Arrowheads represent the peroxisomes interacting with primary cilia, while arrows show the peroxisomes without any contact with cilia. Scale bar, 5 μm.

(F) Quantification of (E) showing that disruption of the *ABCD1* and *NPC1* genes did not alter the number of spatial interactions between peroxisomes and primary cilia for 2 h compared with that of the wild type (one-way ANOVA with Tukey's HSD, n=3: 45–50 peroxisomes per experiment).

(G) Quantification of (E) indicating that disruption of the *ABCD1* and *NPC1* genes did not alter the duration of spatial communication between peroxisomes and primary cilia compared with that of the wild type (one-way ANOVA with Tukey's HSD, n=3: 45–50 peroxisomes per experiment).

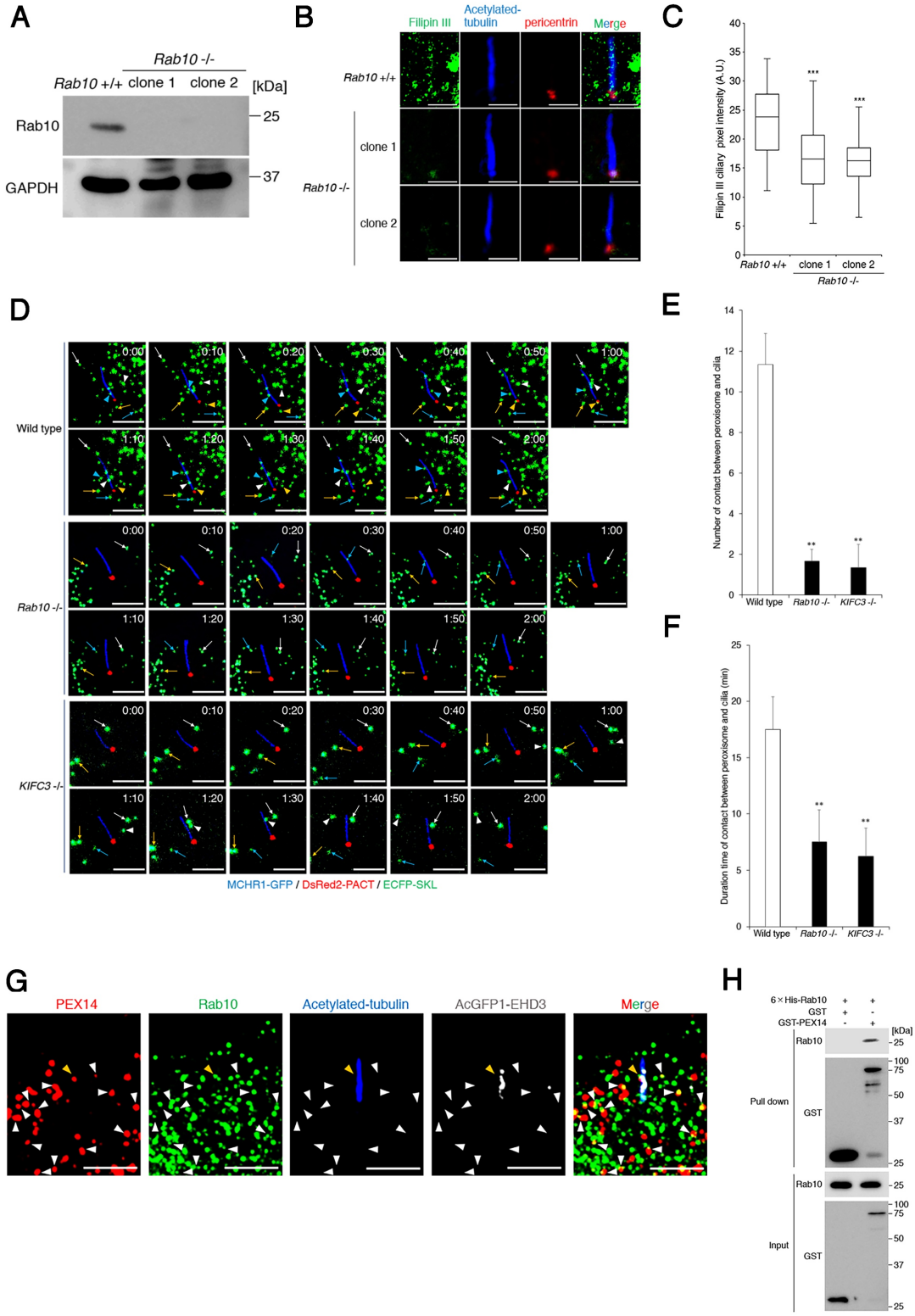

Appendix Fig. S11. The dynamics of peroxisomes for communicating with primary cilia is defective in *Rab10*$^{-/-}$ and *KIFC3*$^{-/-}$ hTERT-RPE1 cells

(A) Western blot analysis showing depletion of Rab10 in the *Rab10*$^{-/-}$ hTERT-RPE1 cell clones. GAPDH served as a loading control.

(B) *Rab10*$^{+/+}$ and *Rab10*$^{-/-}$ hTERT-RPE1 cells incubated for 24 h without serum were immunostained with anti-pericentrin (red) and anti-acetylated-tubulin (blue) antibodies. Cholesterol was stained with Filipin III (green). Scale bar, 5 μm.

(C) Quantification of (B) indicating that *Rab10*$^{-/-}$ hTERT-RPE1 cells significantly reduced the ciliary accumulation of cholesterol (***p<0.001: one-way ANOVA one-way ANOVA with Tukey's HSD, n=3: 40–50 cells per experiment).

(D) Quiescent G_0-phase wild-type, *Rab10*$^{-/-}$, and *KIFC3*$^{-/-}$ hTERT-RPE1 cells transiently expressing MCHR1-GFP (blue), DsRed2-PACT (red), and ECFP-SKL (green) were imaged live for 2 h by confocal microscopy (Movie EV18–20). Arrowheads represent the peroxisomes interacting with primary cilia, while arrows show the peroxisomes without any contact with cilia. Scale bar, 5 μm.

(E) Quantification of (D) showing that disruption of the *Rab10* and *KIFC3* genes significantly reduced the number of spatial interactions between peroxisomes and primary cilia for 2 h (**p<0.01: one-way ANOVA with Tukey's HSD, n=3: 45–50 peroxisomes per experiment).

(F) Quantification of (D) indicating that disruption of the *Rab10* and *KIFC3* genes significantly shortened the duration of spatial communication between peroxisomes and primary cilia (**p<0.01: one-way ANOVA with Tukey's HSD, n=3: 45–50 peroxisomes per experiment).

(G) Confocal images of the quiescent G_0-phase hTERT-RPE1 cells transfected with AcGFP1-tagged EHD3 (white) immunostained with anti-acetylated-tubulin (blue), anti-PMP70 (red), and anti-Rab10 (green) antibodies indicate the Rab10-bound peroxisome (yellow arrowhead) at the ciliary pocket. The white arrowheads show other Rab10-bound peroxisomes. The scale bars indicate 2 μm.

(H) Recombinant GST (0.2 μg) or GST fused to PEX14 proteins (1 μg) and 6×His-Rab10 protein (1 μg) were pulled down using glutathione-Sepharose beads. GST-tagged PEX14 and 6×His-tagged Rab10 proteins in the pull-down fractions and inputs were detected by western blotting.

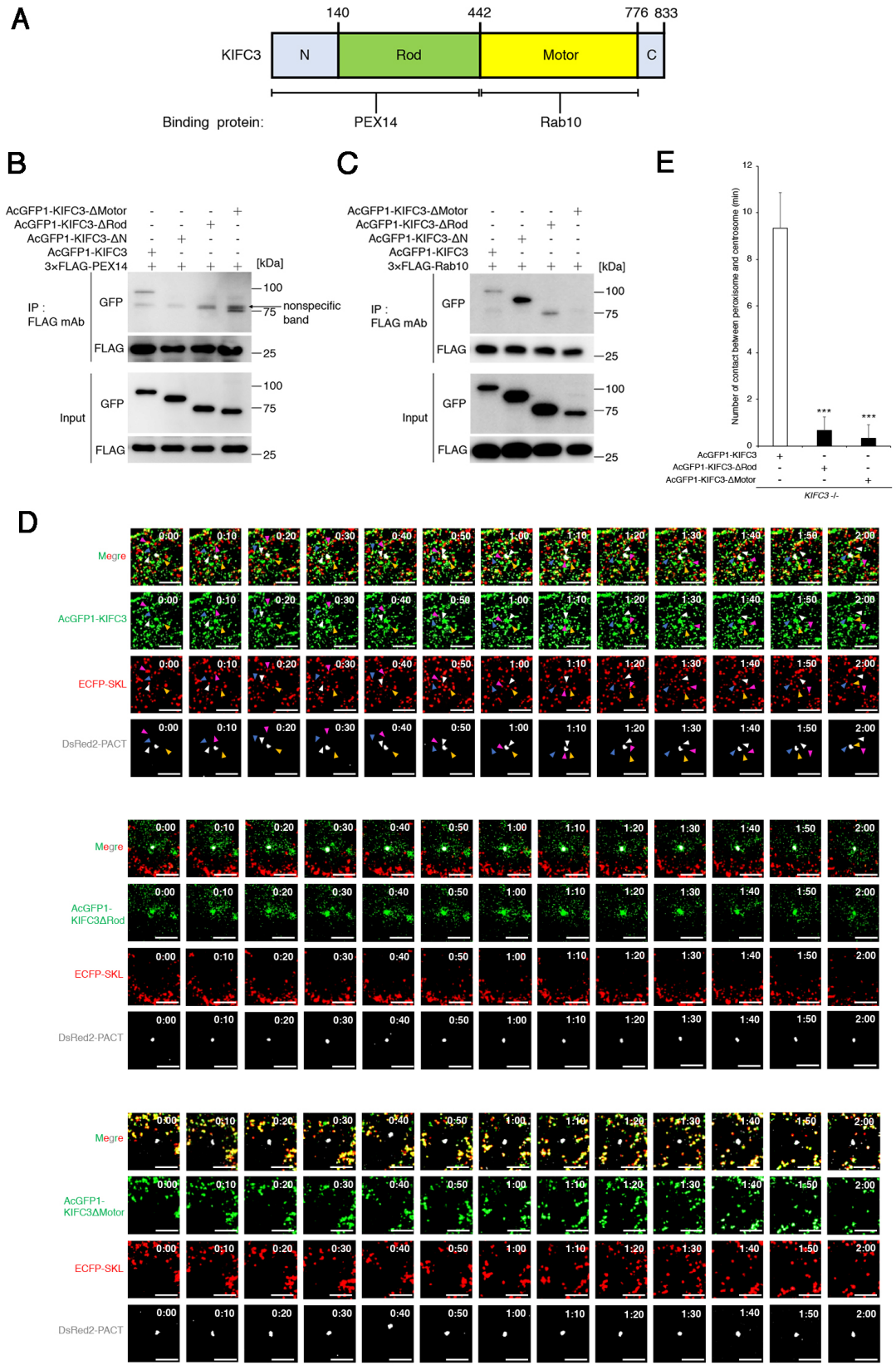

Appendix Fig. S12. KIFC3 physically interacts with Rab10 and Pex14 by its distinct domains

(A) Schematic of KIFC3 structure. KIFC3 is a member of the C-kinesin family characterized by a C-

terminal catalytic motor domain. According to (B) and (C) in Appendix Fig. S5, PEX14 binds to the N-terminal region containing the Rod domain, while Rab10 physically interacts with the motor domain.

(B) Whole-cell lysates from HEK293T cells expressing AcGFP1-tagged KIFC3 or deleted KIFC3 mutants and 3×FLAG-tagged PEX14 were immunoprecipitated with anti-FLAG antibody and immunoblotted with anti-GFP or anti-FLAG antibody.

(C) Whole-cell lysates from HEK293T cells expressing AcGFP1-tagged KIFC3 or deleted KIFC3 mutants and 3×FLAG-tagged Rab10 were immunoprecipitated with anti-FLAG antibody and immunoblotted with anti-GFP or anti-FLAG antibody.

(D) Quiescent G_0-phase *KIFC3*$^{-/-}$ cells transiently expressing AcGFP1-tagged KIFC3, KIFC3ΔRod, or KIFC3ΔMotor (green), DsRed2-PACT (white), and ECFP-SKL (red) were imaged live for 2 h by confocal microscopy (Movie 21–23). Arrowheads represent the AcGFP1-tagged KIFC3-bound peroxisomes interacting with centrosomes. Scale bar, 5 μm.

(E) Quantification of (D) indicating that both AcGFP1-tagged KIFC3ΔRod and KIFC3ΔMotor mutants inhibited the peroxisomal dynamics for communicating with centrosomes (***$p<0.001$: one-way ANOVA with Tukey's HSD, n=3: 45–50 peroxisomes per experiment).

Target genes	Target exones	gRNA and target PAM (5'-NGG-3') sequence	Genotyping primer pairs
PEX1	Exon 13	5'-(CCA)CAAGTCAGTCTCAGCAATCTC-3'	5'-GCTTAATTCCAGCTTTGAATGATATG-3'
			5'-AGTAGTGTATTACCTGATTAGGAGGC-3'
PEX14	Exon 5	5'-ATCATGGCAGGCATTGCATT(TGG)-3'	5'-TTCCCGCCTGTAGGTCCCGCAGGCTC-3'
			5'-TGACTCACCTTGTAGAGCTGGTGAAAGC-3'
Rab10	Exon 3	5'-CTAGTATATGACATCACCAA(TGG)-3'	5'-TTTCAGGGATACAGCAGGCCAGGAGCG-3'
			5'-GGTCTTACCTCATCTATGTTTCTAAGC-3'
Rabin8	Exon 3	5'-AACTAAATTAACTACAAGAA(AGG)-3'	5'-CTTTCATGTTACAGACCCAGCCCCTTG-3'
			5'-GCAAGCCTCTGTTATAGTAGCACCCTG-3'
ABCD1	Exon 3	5'-TGCCCGCAACCTCCTGACAG(CGG)-3'	5'-ATGCAGAGGCCGTGAAGAAGGCAGCCTTG-3'
			5'-CTCCTTGTACGACGACATGATCCGCTC-3'
NPC1	Exon 9	5'-CCAGAACAGCCATTCCGTGC(TGG)-3'	5'-CAGGTTCTTGACTTACAAATAGCCATCG-3'
			5'-GTGGTAATCGGCATACACAAAGAAGTCG-3'
KIFC3	Exon 11	5'-(CCA)CCAATGCTGTGACTTTCGAT-3'	5'-GGAACATCCGAGTGATTGCTCGTGTCCG-3'
			5'-GTCCTGCTGCGAGGCCTGTGGGGAGAAG-3'
EHD1	Exon 3	5'-GCTCTTCGACGCCCACAAGC(TGG)-3'	5'-GCTATGACTTTGCAGCCGTCCTGGAGTG-3'
			5'-GTCTCGATCTGGTCTGCCTTGTTCAGCAC-3'
EHD3	Exon 2	5'-GACATGGAGGGGATCATCCC(TGG)-3'	5'-GTACCTGCTGGAACAGGACTTCCCAG-3'
			5'-CTGTTCAAGAAGGCGTTGCCAAAGGC-3'
ORP3	Exon 6	5'-(CCA)TGTTTCCACATGAAGTTAAC-3'	5'-GTCAAGTCAGAAGAAGTCTTTGATGAG-3'
			5'-CTTCCTACTTGAAATGGAGTCAAACACC-3'
mouse *PEX14*	Exon 3	5'-TCCTACAGAATTCTCGGGTC(CGG)-3'	5'-TCCCCTACCAGATTGCCACAGCAGTG-3'
			5'-CTGCCAAGGAAACCTGTACCTTTCTTC-3'

Appendix Table S1. Target genomic sites in hTERT-RPE1 cells for the CRISPR-ObLiGaRe-mediated gene knockout

Cell line ID	target exon	Allele 1 (ObLiGaRe-mediated *NeoR* cassette integration)	Allele 2 (CRISPR/Cas9-mediated indel mutations)	
			DNA sequence alteration	Amino acid alteration
ABCD1 -/- clone 1 (hTERT-RPE1)	*ABCD1* exon 3	*NeoR* (+) : Reverse integration	c.1173 del CTGA	L392fs
ABCD1 -/- clone 2 (hTERT-RPE1)	*ABCD1* exon 3	*NeoR* (+) : Forward integration	c.1177 ins A	T393fs
EHD1 -/- clone 1 (hTERT-RPE1)	*EHD1* exon 3	*NeoR* (+) : Reverse integration	c.617 del TG	H206fs
EHD1 -/- clone 2 (hTERT-RPE1)	*EHD1* exon 3	*NeoR* (+) : Reverse integration	c.620 ins T	L208fs
EHD3 -/- clone 1 (hTERT-RPE1)	*EHD3* exon 2	*NeoR* (+) : Forward integration	c.326 ins >100bp	P110fs
EHD3 -/- clone 2 (hTERT-RPE1)	*EHD3* exon 2	*NeoR* (+) : Reverse integration	c.326 ins T	I109fs
KIFC3 -/- clone 1 (hTERT-RPE1)	*KIFC3* exon 11	*NeoR* (+) : Forward integration	c.1466 ins A	N467fs
KIFC3 -/- clone 2 (hTERT-RPE1)	*KIFC3* exon 11	*NeoR* (+) : Forward integration	c.1466 ins A	N467fs
NPC1 -/- clone 1 (hTERT-RPE1)	*NPC1* exon 9	*NeoR* (+) : Forward integration	c.1481 ins A	S493fs
NPC1 -/- clone 2 (hTERT-RPE1)	*NPC1* exon 9	*NeoR* (+) : Reverse integration	c.1481 ins A	S493fs
ORP3 -/- clone 1 (hTERT-RPE1)	*ORP3* exon 6	*NeoR* (+) : Forward integration	c.1481 ins T	Q713fs
ORP3 -/- clone 2 (hTERT-RPE1)	*ORP3* exon 6	*NeoR* (+) : Forward integration	c.466 ins T	P156fs
PEX1 -/- clone 1 (hTERT-RPE1)	*PEX1* exon 13	*NeoR* (+) : Forward integration	c.466 ins T	P156fs
PEX1 -/- clone 2 (hTERT-RPE1)	*PEX1* exon 13	*NeoR* (+) : Reverse integration	c.2135 ins A	S712fs
PEX14 -/- clone 1 (hTERT-RPE1)	*PEX14* exon 5	*NeoR* (+) : Reverse integration	*NeoR* (+) : Reverse integration	NeoR replacement
PEX14 -/- clone 2 (hTERT-RPE1)	*PEX14* exon 5	*NeoR* (+) : Reverse integration	c.361 ins > 200 bp insertion	F121fs
Rab10 -/- clone 1 (hTERT-RPE1)	*Rab10* exon 3	*NeoR* (+) : Reverse integration	c.276 ins C	N93fs
Rab10 -/- clone 2 (hTERT-RPE1)	*Rab10* exon 3	*NeoR* (+) : Reverse integration	c.276 del C	N93fs
Rabin8 -/- clone 1 (hTERT-RPE1)	*Rabin8* exon 3	*NeoR* (+) : Forward integration	c.370 ins A	R124fs
Rabin8 -/- clone 2 (hTERT-RPE1)	*Rabin8* exon 3	*NeoR* (+) : Forward integration	c.370 ins A	R124fs
PEX14 -/- clone 1 (NIH3T3)	mouse *PEX14* exon 3	*NeoR* (+) : Reverse integration	c.116 del TCGGGTCCGGC	S39fs
PEX14 -/- clone 2 (NIH3T3)	mouse *PEX14* exon 3	*NeoR* (+) : Reverse integration	c.121 del G	R40fs

Appendix Table S2. Genotypes of the edited hTERT-RPE1 cell lines using the CRISPR-ObLiGaRe method